Solids flow patterns in large-scale circulating fluidised bed boilers: Experimental evaluation under fluid-dynamically down-scaled conditions

Chemical Engineering Science xxx (xxxx) xxx

Contents lists available at ScienceDirect

Chemical Engineering Science

journal homepage: www.elsevier.com/locate/ces

Solids flow patterns in large-scale circulating fluidised bed boilers: Experimental evaluation under fluid-dynamically down-scaled conditions

Tove Djerf *, David Pallarès, Filip Johnsson

Department of Space, Earth and Environment, Chalmers University of Technology, 412 96 Göteborg, Sweden

HIGHLIGHTS

- Cold flow model according to scaling laws and resembling a 200 MWth CFB boiler.
- Validation of down-scaled unit showed good similarity with reference boiler.
- Vast experimental evaluation of solids flow pattern in CFB boilers.
- The presence or absence of a dense bed governs the entrainment of solids.
- Solids external circulation should not be estimated as the solids flux at riser top.

ARTICLE INFO

Article history:
Received 10 August 2020
Received in revised form 5 November 2020
Accepted 12 November 2020
Available online xxxx

Keywords:
Circulating fluidised bed
Fluid-dynamical scaling
Solids flow pattern
Dense bed
Solids entrainment

ABSTRACT

This work aims at gaining novel knowledge of the mechanisms governing the solids flow pattern in the furnace of large-scale Circulating Fluidised Bed (CFB) boilers. A fluid-dynamically down-scaled unit resembling an existing 200-MW_{th} CFB boiler was built and validated against full-scale data. The extensive experimental campaign showed, among others, that the presence or absence of a dense bed governs the entrainment of solids from the bottom region of the furnace, and that the back-flow of solids at the exit region is negligible at low gas velocities although it quickly becomes significant with an increase in gas velocity. Thus, it is shown that the estimation of the external solids flux by the top flux in the furnace is not generally valid.

1. Introduction

The circulating fluidised bed (CFB) is an established technology for the large-scale combustion of solid fuels in boilers (Koornneef et al., 2007; Cai et al., 2018). It provides, among other things, inherent control of polluting emissions (Koornneef et al., 2007; Cai et al., 2018; Leckner, 1998) and high fuel flexibility and, thus, the possibility for decreased use of fossil fuels by introducing biomass and/or renewable waste as fuel (Koornneef et al., 2007; Minchener, 2003). The introduction of renewable electricity generation from non-dispatchable technologies, such as wind and solar power, has made load flexibility a highly valuable feature, both in terms of minimum load and load-ramp rates (Huttunen et al., 2017). This increases the need for knowledge on the optimisation of design and operation, as well as a better understanding of the increased flexibility of combined heat and power plants.

Given the complex nature of the in-furnace processes in CFB boilers with their two-phase gas solids flow, much of our current knowledge of CFB has been acquired from experimental data (see, for example (Johnsson and Leckner, 1995; Werdermann, 1993; Couturier et al., 1991; Johnsson et al., 1995; Lafanechere and Jestin, 1995; Leretaille et al., 1999; Johansson, 2005; Mirek, 2016; Yang et al., 2005)). This is because modelling from first principles either requires too great a computational effort (for a Lagrangian description of each solid particle) or entails terms with high levels of uncertainty in the governing equations (Eulerian description of the solids phase). Experimental knowledge is typically used to build semi-empirical models (Myöhänen, 2011; Hannes, 1998; Pallarès, 2008; Wischnewski et al., 2010), which have shown satisfactory reliability and affordable computational costs. However, the validity of the semi-empirical expressions is

* Corresponding author.
E-mail address: tovek@chalmers.se (T. Djerf).

https://doi.org/10.1016/j.ces.2020.116309
0009-2509/

Nomenclature

Notations

a	decay coefficient of the splash zone [1/m]
A_{**}	cross-sectional area [m^2]
D	equivalent riser diameter [m]
d_p	particle diameter [μm]
g	gravity constant, 9.81 m/s^2 [m/s^2]
G_s	external circulation of solids [kg/m^2s]
$G_{s,**}$	solids flux [kg/m^2 s]
h	height over distributor plate [m]
H_b	dense bed height [m]
H_{exit}	exit height of the riser [m]
k	net mass transfer coefficient [m/s]
K	decay coefficient of the transport zone [1/m]
k_b	back-flow ratio [–]
L	length [m]
L^*	scale factor for length [–]
m^*	scale factor for mass [–]
p^*	scale factor for pressure [–]
PSD	particle size distribution [–]
St	Stokes number [–]
t^*	scale factor for time [–]
u^*	scale factor for velocity [–]
u^{**}	fluidisation velocity [m/s]
u_0	fluidisation velocity [m/s]
$u_{L^{**}}$	secondary air velocity at top riser cross section [m/s]
u_{mf}	minimum fluidisation velocity [m/s]
u_t	terminal velocity [m/s]
δ_b	bubble fraction [–]
ΔP_{**}	pressure drop [Pa]
μ_g	viscosity [Pas]
ρ_{**}	density, concentration [kg/m^3]
$\rho_{s,**}$	solids concentration in ** [kg/m^3]
$\rho_{s,entr}$	concentration of entrained solids from bottom region [kg/m^3]
Φ	particle sphericity [–]

Subscript **

seal	value in particle seal
b	dense bed
DC	down-comer
down	downwards motion
exit	values at the exit zone
g	gas
Hb	values at the dense bed
L.1	height L.1
L.2	height L.2
p	particle
Ref	reference values measured in the range of h = 0.1–1.6 m
Riser	riser, values measured for h = 0.1 m - top of the riser
s	solids
top	value at the top of riser
Gs,valve	values at the solids circulation valve

obviously limited to the geometrical and operational range of the measurement data from which they were originally derived.

The solids flow is a key aspect of the design and operation of CFB combustion, as it governs the mass balance of the bed material and it may also be active in the mass balance of the gas phase when serving as a catalyser or sorbent, for example, for the in-bed capture of pollutant emissions. In addition, the solids flow influences the mass, momentum and heat transfer to fuel particles, as well as the heat balance across the circulating loop, thereby determining the enthalpy flows of the solids and the heat transfer coefficients. More specifically, the external circulation of solids is an important parameter because it allows for heat extraction in the return leg, which acts as a mechanism to control the temperature level in the hot loop. The external heat exchanger in the return leg can, therefore, extend the range of operation of CFB boilers.

Despite being essential for a fundamental understanding of commercial CFB boilers, the measured data from large-scale units are relatively scarce, being typically limited in terms of spatial resolution and operational range. Measurements conducted in smaller CFB units have been important but have typically been carried out under conditions that are not necessarily relevant for CFB boilers. In particular, much of the data available in literature have been acquired under ambient conditions in tall and narrow risers with geometries quite different from those of CFB boiler furnaces, which are characterised by a height-to-width ratio of the order of ≤ 10 (Johnsson et al., 1995). As a consequence, it is not obvious to what extent – if any – the results reported in the literature for narrow units can provide information that can be applied to the understanding and modelling of CFB furnaces.

The over-arching aim of this work was to elucidate the underlying macroscopic mechanisms governing the solids flow patterns in the furnaces of large-scale CFB boilers. The specific goals were to develop an understanding of how different variables affect the entrainment of solids from the furnace bottom region, their backmixing along the furnace walls, and their back-flow in the exit region at the top of the furnace.

To achieve these aims, a fluid-dynamically down-scaled unit of an existing large-scale (~200-MW_{th}) CFB boiler was built. Data from the down-scaled unit was successfully validated against measurements from the large reference CFB boiler. The influences of several parameters on the solids flow were investigated in terms of the fluidisation velocity, riser pressure drop, and secondary air injected at two height levels. Special emphasis was placed on determining the flow conditions at the bottom of the riser, i.e., the furnace, and on evaluating the conditions corresponding to partial-load operation.

2. Theory

CFB units are used in a wide range of applications (Kunii and Levenspiel, 1991), with several studies in the literature focusing on fluid catalytic cracking (FCC) units, which have narrower risers than the furnaces of CFB boilers (Leckner, 2017). Large-scale CFB boilers are run with Geldart B group solids and a dense bottom region with a low (much less than 1) height-to-width aspect ratio. These boilers exhibit a lateral solids flux profile in the freeboard that is almost flat and they yield solids net flux values that are typically in the range of 0.5–20 kg/m^2s. In contrast, FCC units use Geldart group A particles, have a height-to-width aspect ratio > 1 in their denser bottom region, show a solids profile in the freeboard that is parabolic in shape, and employ a much higher net solids flux than that used in CFB boilers (Johnsson et al., 1995; Zhang et al., 1991).

2.1. Solids flow in wide CFB risers

According to the description of the vertical solids concentration profile given by Johnsson and Leckner (1995), the riser of a CFB boiler can be divided into three different fluid dynamical zones: a dense bottom bed, a splash zone, and a transport zone (see Fig. 1). In addition, there is a more- or less-pronounced exit zone in connection to the outlet to the cyclone.

This division of the freeboard flow into a splash and a transport zone has been validated in different large-scale CFB boilers (Pallares and Johnsson, 2006; Schouten et al., 1999) and is considered to be an improvement upon previous correlations in which the freeboard (i.e., splash and transport zone) was expressed as a single region (Löffler et al., 2003). Despite the significant upward net flux of solids from the bottom region, and application of primary gas velocities, which typically exceed the terminal velocity, there is evidence of a dense bottom bed above the primary gas distributor with fluid-dynamics similar to that of a bubbling bed, with a constant pressure drop, i.e., a constant solids concentration (Johnsson et al., 1991); ρ_{s,H_b} with height, H_b (Leckner, 2017). Yet, the presence of such a dense bed has only been observed in the Chalmers boiler due to its densely spaced pressure taps (Svensson et al., 1996). Most commercial CFB boilers have too few pressure taps to allow confirmation of the presence of a dense bed according to the above definition.

The splash zone is dominated by strong back-mixing, manifested as the ballistic movement of clustered particles. These clusters are ejected via bubble eruptions at the dense bed surface. The strong back-mixing results in a steep decrease in the solids concentration with height, which is described by an exponential decay coefficient, a (Kunii and Levenspiel, 1990). The transport zone, which is located above the splash zone, occupies most of the riser height and is populated by those particles that are entrained from the bottom region (the dense bed and the splash zone). The transport zone consists of an upwards core flux with back-mixing through the separation of solids to the riser walls, forming a solids wall layer that is flowing downwards. The solids back-mixing to the wall layers is described by a decay coefficient, K.

From the integration of the solids-flux mass balance across a height segment of the furnace, the vertical profile of solids concentration can be described by Eq. (1) (Johnsson and Leckner, 1995):

$$\rho_s(h) = \rho_{s,H_b} \quad h < H_b \tag{1.1}$$

$$\rho_s(h) = \left(\rho_{s,H_b} - \rho_{s,exit} e^{K(H_{exit}-H_b)}\right) e^{-a(h-H_b)} + \rho_{s,exit} e^{K(H_{exit}-h)} \quad H_b < h < H_{exit} \tag{1.2}$$

While the literature contains models and expressions for ρ_{s,H_b}, (Pallares and Johnsson, 2006; Gómez-Barea and Leckner, 2010); a (Johnsson and Leckner, 1995) and K (Johnsson and Leckner, 1995; Davidson, 2000), the solids concentration at the top of the riser, $\rho_{s,exit}$ is not as straight-forward to describe, as it also depends on the exit geometry of the furnace. Combining the expressions of Johnsson and Leckner (1995), and the original works of Wen and Chen (1982) and Kunii and Levenspiel (1990) for a dispersed flow of particles entrained from the bottom bed, we define the concentration of the solids entrained from the bottom bed, $\rho_{s,entr}$ (see Fig. 1). Thus, $\rho_{s,entr}$ corresponds to the concentration obtained from the extrapolation of the upper concentration profile – analogous to the upwards moving dispersed phase - down to the dense bed height, H_b (or, in the absence of a dense bed, down to the bottom grid) (see Fig. 1) (Karlsson et al., 2017; Djerf et al., 2018). From this, the vertical profile of the solids concentration can be written as:

$$\rho_s(h) = \left(\rho_{s,H_b} - \rho_{s,entr}\right) e^{-a(h-H_b)} + \rho_{s,entr} e^{-K(h-H_b)} \quad h > H_b \tag{1.3}$$

where $\rho_{s,entr}$ can be obtained from experiments.

The decay coefficient in the transport zone, K, has been described as a function of the solids transport velocity as $K = A/(u_0\text{-}u_t)$ (Johnsson and Leckner, 1995), which in turn can be expressed as a function of the net mass transfer coefficient between the core and annular region, k, by setting $A = 4\ k/D$ (Davidson, 2000). Thus, the decay coefficient is dependent upon the cross-sectional size and aspect ratio of the riser. Although mea-

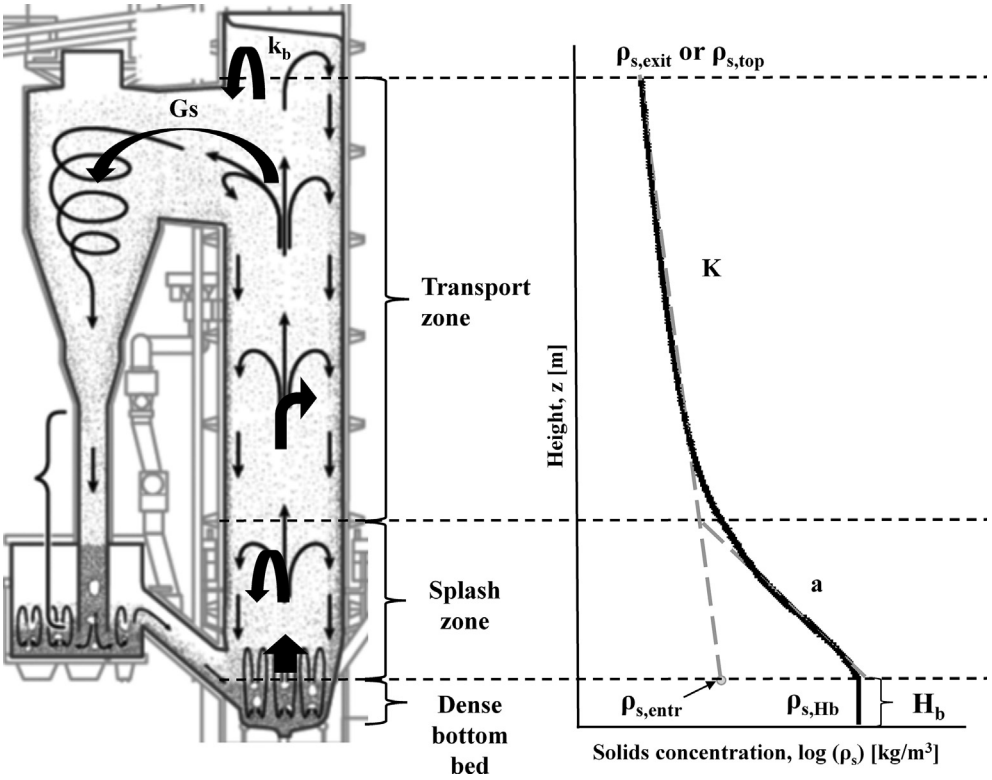

Fig. 1. Schematic of the different fluid-dynamical zones in the riser of a CFB boiler according to Johnsson and Leckner (1995), including a typical vertical profile of solids concentration together with the key parameters used in the mathematical description provided by Johnsson and Leckner.

surements made in the Chalmers 12-MW_{th} CFB boiler yielded a value of $A = 0.23\ s^{-1}$ (Johnsson and Leckner, 1995), the expression for A indicates a dependency on furnace geometry.

The upwards core flux of solids at the top of the riser, $G_{s,top}$, can be calculated as:

$$G_{s,top} = \rho_{s,top}(u_0 - u_t) \tag{2}$$

The external circulation of solids is often estimated to be equal to the upwards core flux of solids in the top (Johnsson and Leckner, 1995; Werdermann, 1993; Zhang et al., 1995; Johansson et al., 2007). However, studies show that there can be significant solids back-mixing at the riser exit, also known as *back-flow effect* (Pallares and Johnsson, 2006; Johansson et al., 2007; Senior and Brereton, 1992; Van der Meer et al., 2000; Werther, 1993). This involves a share of the solids flowing upwards at the exit height not being circulated externally, but instead being internally recirculated through the wall layers. Thus, with the back-flow ratio defined as $k_b = G_{s,down}/G_{s,top}$ and noting that $G_{s,down} = G_{s,top}$-G_s, the externally circulated solids flux can be expressed as:

$$G_s = (1 - k_b)G_{s,top} \tag{3}$$

Werther (1993) estimated that the back-flow ratio under three specific operational cases in three large CFB boilers was approximately 0.2. Furthermore, the geometry of the riser exit/top configuration has been found to influence the back-flow ratio (Van der Meer et al., 2000; Werther, 1993; Johnsson et al., 1999), with for example, a specific abrupt exit yielding a 30% higher back-flow compared to a smooth exit (Werther, 1993), an effect that is enhanced at higher solids concentrations (Pallares and Johnsson, 2006). However, experiments that have applied different exit configurations for conditions similar to those typical of CFB boilers (relatively low solids fluxes) revealed a weak influence of the exit configuration (Johnsson et al., 1999). The back-flow effect was only affected significantly when large internals were inserted in the upper part of the furnace, partly blocking the exit to the cyclone. Analysis of the measurements made in the Chalmers 12-MW_{th} CFB boiler have shown that finer particles experience lower back-flows than coarser ones and that, as expected, higher solids concentrations increase the back-flow (Pallares and Johnsson, 2006). It can be concluded that although the back-flow effect depends on the design of the upper part of the furnace, the solid flux condition and particle size may also influence the solids concentration at the top of the furnace.

Regarding the external circulation of solids, its measurement in large-scale units represents a major challenge. Edvardsson et al. (2006) have estimated the external circulation of solids in a CFB boiler by solving a heat balance over a loop seal system equipped with a heat exchanger. Yue et al. (2005) have gathered data on solids circulation from nine large-scale CFB boilers, although it is not fully clear how these values (all but one is <12 kg/m^2s) were measured/estimated. In addition, care should be taken when comparing solids circulation rates from different units, as several unit-specific variables (e.g., riser height and cross-sectional dimensions, secondary air location, tapered walls, inclination) are known to influence the solids circulation rate. Some studies have shown that the external solids circulation rate is dependent upon the solids inventory, while others have shown the opposite (Yue et al., 2005; Yang et al., 2009; Xu et al., 2015). Nonetheless, recent studies (Karlsson et al., 2017; Djerf et al., 2018) have revealed that the increase in the external circulation rate of solids that occurs with increased gas velocity levels off when the dense bottom bed is depleted. Furthermore, the same studies have shown that in the absence of a dense bottom bed, the external circulation of solids increases with the solids inventory, whereas if a dense bed is present the external circulation is not affected by the solids inventory (at a constant velocity).

While secondary air injections are used to decrease NO_x emissions and to control the temperature in the bottom region, they also influence the external circulation of solids (Cho et al., 1994). Studies conducted in smaller, laboratory-scale units (Zheng et al., 2019) have found that secondary air injection hinders the entrainment of solids, thereby yielding a lower solids concentration at the top of the riser (and, thus, an increased concentration of solids below the secondary air inlet, given the same riser pressure drop). It should be noted that the data in (Zheng et al., 2019) were generated by maintaining the total gas flow constant and varying the primary-to-secondary air ratio, resulting in a decrease flow of primary air when the secondary air was increased. Therefore, it is difficult to compare these results to those of laboratory-scale units (Zheng et al., 2019). Nevertheless, measurements from one case in the Chalmers 12-MW_{th} boiler showed that secondary air injection increased the solids concentration in the upper part of the furnace above the point of secondary air injection, when the primary air flow was kept constant (Johnsson and Leckner, 1995). Thus, it can be concluded that the influence of secondary air on the solids flow remains unclear.

2.2. Fluid-dynamical scaling laws

Fluid-dynamical scaling allows one to study the fluid dynamics of large, high-temperature units using smaller laboratory units that are operated under ambient conditions, without losing the quantitative relevance of the measured data. Applying laboratory units that are operated according to scaling laws also enables investigations with a greater range of operational parameters than is possible in full-scale boilers and the use of a wider range of diagnostic techniques. The scaling is based on identifying dimension-less parameters and ensuring that they are equal in the reference and the laboratory unit (Kalaga et al., 2020). For fluid-dynamical down-scaling of fluidised beds, Glicksman (1984) has proposed initially a full set of scaling parameters (used in (Markström and Lyngfelt, 2012; Glicksman et al., 1994) for which the length scale-factor, L^*, is given by the gas chosen to operate the cold flow model. In our case (FB combustion resembled with ambient air), this results in L^*=0.22, which will obviously yield a too-large cold flow model to fit in the laboratory space.

The following simplified scaling laws have been presented by Glicksman et al. (1993):

$$\frac{u_0^2}{gD}, \frac{\rho_p}{\rho_g}, \frac{u_0}{u_{mf}}, \frac{L}{D}, \frac{G_s}{\rho_p u_0}, \varnothing, PSD \tag{4}$$

Horio et al. (1989) had earlier presented a set of scaling laws similar to Eq. (4), with u_t substituting for u_{mf} in the third dimension-less group (Van der Meer et al., 1999). This results in only minor variations to the resulting scaling. Combining the first and third groups in Eq. (4), the length scaling factor for the simplified set becomes:

$$L^* = \frac{L_{cold}}{L_{hot}} = \left(\frac{u_{mf}]_{cold}}{u_{mf}]_{hot}}\right)^2 \tag{5}$$

Thus, given a gas velocity in the cold flow model, the length scale factor can still be adjusted through varying the particle size [the solids density is given by the second group in Eq. (4)], with finer solids yielding smaller cold flow models. However, it should be noted that for finer solids other forces, e.g., inter-particle forces and static charging, may also affect the solids flow. In this sense, it is crucial to keep the scaled solids with in the same Geldard group as the reference solids. The flexibility offered by the simplified set for designing cold flow models has turned it into a widely used tool

in the field of fluidisation (Van der Meer et al., 2000, 1999; Johnsson et al., 1999; Glicksman et al., 1993; Sette et al., 2014; Schöny et al., 2016; Sasic et al., 2004).

Among the possibilities for further simplification of the scaling sets, Van der Meer et al. (1999) have proposed to omit $\frac{\rho_p}{\rho_g}$, which Glicksman validated experimentally for very low values of Re_p (Leckner et al., 2011), thereby creating the opportunity to choose the particles more freely and avoid issues with high-density particles. However, Van der Meer et al. (1999) noted that this approach maintains only approximately the fluidisation regime and macroscopic movement of the solids, as well as the riser solids volumetric hold-up, while the mass and pressure drop similarities are lost.

Finally, in the case of large-scale CFB boilers, the external circulation of solids, G_s, is not an externally controllable (or known) parameter but is the result of boiler operation and design. Thus, the solids circulation can be controlled by adjusting the mass of solids in the system, as represented by the riser pressure drop. So, when scaling large-scale CFB boilers the fifth dimension-less group in Eq. (4) that represents the external solids circulation has to be substituted with the dimension-less riser pressure drop, $\Delta p/\rho_p gL$.

3. Experiments

Based on the simplified set of scaling laws described by Glicksman et al. (1993) in Eq. (4), a fluid-dynamically down-scaled unit was built to resemble an existing ~200-MW_{th} CFB boiler – hereinafter termed the 'reference boiler'.

3.1. Fluid-dynamical down-scaling

Using air at ambient temperature as the fluidisation agent implies, via the second dimension-less group in Eq. (4), the use of a high-density bed material; copper is chosen (8920 kg/m^3 compared to a target value of 9375 kg/m^3). As the next step, a length scaling factor of 1/13 was judged to be optimal, since it resulted in a fluid-dynamically down-scaled unit with a height of 3 m. In order to achieve this, a particle size of 35 μm is required [see Eq. (5)], which yields Geldart B solids, i.e., the same as the solids in the reference boiler. This scaling (see Table 1 for values and scaling factors) resulted in an error of 5% in the second dimension-less group in Eq. (4), i.e., the solids-to-gas density ratio, while the remaining four first groups in Eq. (4) were maintained in full agreement by adjusting the fluidisation velocity, particle size and unit dimensions.

The sphericity of the particles [the sixth dimension-less group, see Eq. (4)] is not measured in either the reference boiler or the fluid-dynamically down-scaled unit. The solids in the reference boiler are mainly make-up material and fuel ash (which have undergone attrition) and are typically assigned sphericity values of around 0.85 in the literature. The atomic-blown copper particles used in the cold flow model also tend to be spherical and are assumed to have a sphericity close to that of the solids in the reference boiler.

As for the particle size distribution (PSD) of the solids, in CFB boilers it is determined by the solids flow combined with the solids attrition and cyclone efficiency. Since the latter two factors would be complex to scale effectively, the approach taken here is to fill the cold flow model with solids such that the scaled PSD corresponds to the resulting solids inventory in the boiler, and to use an efficient cyclone that keeps the material in the loop. However, determining the solids PSD in large CFB boilers is problematic, as *in situ* bed solids sampling is required. This sampling should preferably be conducted at different locations in the CFB loop due to the size segregation effects. In the present work, samples of the solids were taken from the loop seal in the reference boiler when it was operated under high-circulation conditions and analysed using laser diffraction, yielding an average size of $d^{50}_{p,boiler}$ = 190 μm. The fresh copper powder used in the fluid-dynamically down-scaled unit has, on an up-scaled basis, an average particle size of $d^{50}_{p,upscaled}$ = 175 μm, which is considered to be in satisfactory agreement with the corresponding value for the reference boiler.

Finally, the air distributor plate and the air feeding system were designed to yield a pressure drop curve and volume, respectively, resembling on an up-scaled basis the reference boiler. This is the case because the pressure drop across the air distributor plate and the volume of the air feeding system have been shown to influence strongly the fluid-dynamics (see (Svensson et al., 1996) and (Sasic et al., 2004), respectively), for the limited air-distributor pressure drops cases, which are typical for boilers.

3.2. Experimental set up

The riser is built of perplex glass to allow direct visual observations of the solids flow. The present work applies tapered walls to the cold flow model for validating the measurements against those in the reference boiler (which has tapered walls), although the measurement campaign after validation applies a bottom section with vertical walls to simplify the flow picture and analysis. The riser roof was kept in a horizontal position for both the validation tests and the research test campaign, despite the slightly inclined roof of the reference boiler.

Fig. 2 shows that the air feeding system consists of two inlet fans and one suction fan, which ensure that the solids loop is below atmospheric pressure so as to prevent solids leakage. The primary and secondary air flows are monitored with three flow-meters and regulated with four valves through a LabView interface. The secondary air can be injected at two height levels (L.1 and L.2). Auxiliary air flows (loop seal fluidisation, purging of pressure taps, cleaning of particle filter) are fed with a separate pressurised air system.

Table 1
Scaling parameters used in this work.

Parameter		Reference boiler	Fluid-dynamically down-scaled unit	
Density of fluidisation gas	ρ_g	0.33	1.2	kg/m^3
Dynamic viscosity of the fluidisation gas	μ_g	4.28E−05	1.81E−05	Pa s
Particle density	ρ_p	2600	8920	kg/m^3
Average particle size	d_p	190	35	μm
Minimum fluidisation velocity	u_{mf}	0.016	0.0045	m/s
Length	L*	L	0.077L	m
Velocity	u*	u	0.277u	m/s
Time	t*	t	0.277t	s
Mass	m*	m	0.00165m	kg
Pressure	p*	p	0.278p	Pa

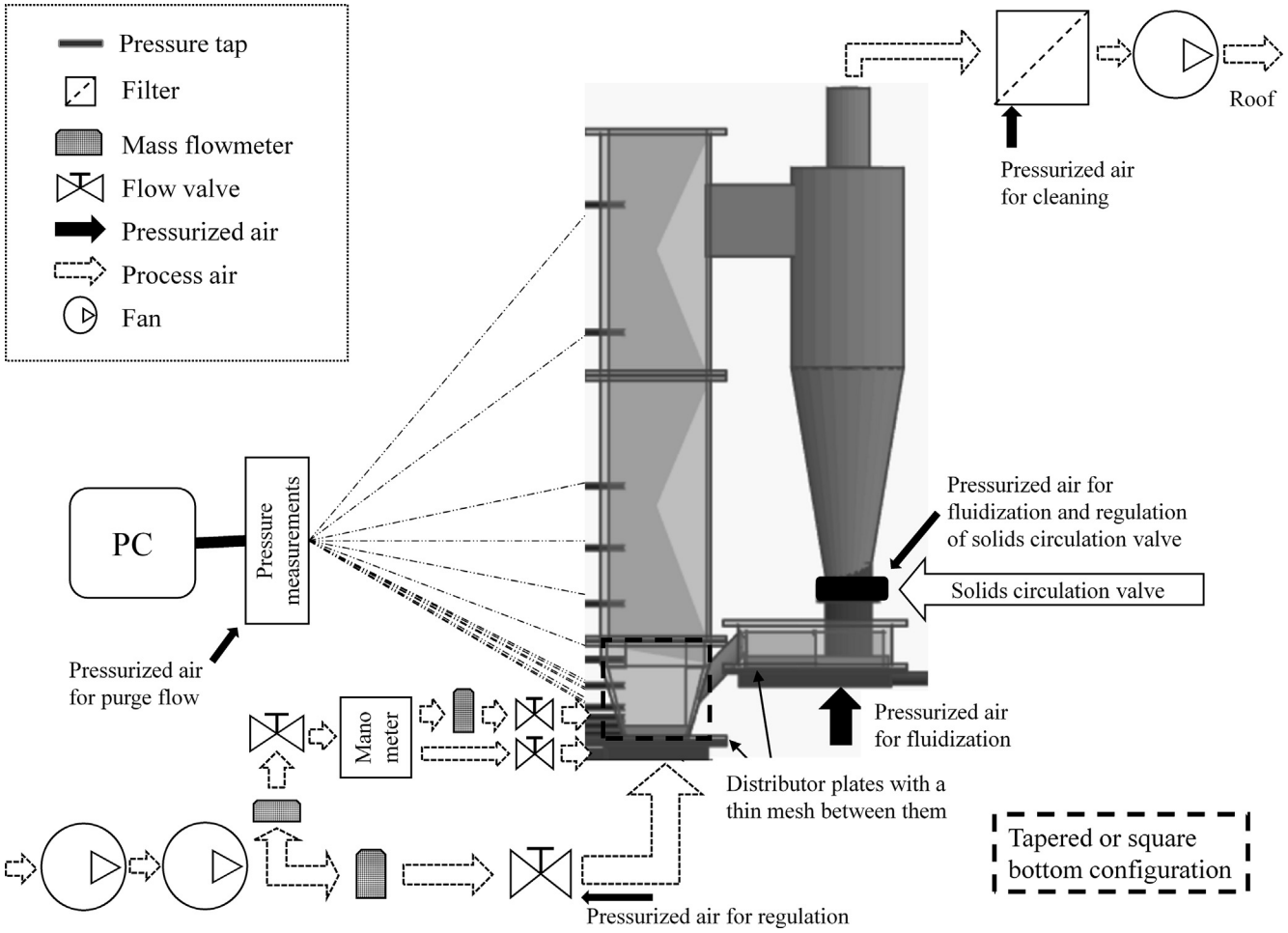

Fig. 2. Layout of the experimental set-up. Two different configurations of the lower section of the furnace were used: one with vertical walls (main measurement campaign) and one with tapered walls (for validation against the reference boiler).

The air distributor is a perforated plate with the locations of each hole corresponding to those of the nozzles in the reference boiler. The need for a relative low pressure drop across the air distributor means that there are relatively large holes in the air distributor ($>d_{p,down\text{-}scaled}^{50}$), requiring the use of two plates with a thin metal mesh inserted in-between them in order to avoid leakage of solids down into the air plenum. At 3.5 m/s, the pressure drop across the air distributor for the reference boiler is 5 kPa, while the fluid-dynamically down-scaled unit yields a value of 5.4 kPa (up-scaled basis), which is considered a satisfactory level of agreement.

To ensure that the copper solids maintain the PSD, the cyclone in the cold flow model is not scaled but is instead specially designed for maximal capture efficiency. For the chosen copper solids, the cyclone manages to keep, after long-term operation, 99.97% of the initial inventory within the CFB loop.

The riser of the fluid-dynamically down-scaled unit is equipped with 15 piezoelectric pressure sensors along the riser height. A total of 7 sensors are situated within a height of 1 m (on an up-scaled basis) above the air distributor in order to enable a higher resolution of the pressure profile in the bottom region than that available in large CFB boilers. The sensors were calibrated prior to the experimental campaign and have shown robust signal repeatability during the experiments. From the pressure measurements the concentrations of solids, $\rho_s(1-\varepsilon_g)$, is derived as (Johnsson et al., 1991; Sasic et al., 2007):

$$\Delta P = \left(\left(\rho_s - \rho_g\right)(1-\varepsilon_g) + \rho_g\varepsilon_g\right)g\Delta h \tag{6}$$

Eq. (6) is applicable down to low solids concentrations, although it neglects acceleration effects (Sasic et al., 2007). Besides the riser, pressure is also sampled in the air plenum, the cyclone outlet, the down-comer, and the particle filter after the cyclone. The solids circulation valve in the down-comer in Fig. 2 consists of a butterfly valve (Djerf et al., 2018), which is used for measuring the external circulation of solids, as explained below.

3.3. Experimental procedure

For each run, pressure measurements are sampled at 50 Hz during a period of 2 min, which is sufficient to give robust statistics. Between runs, the pressure taps are flushed with air to ensure that there are no particle plugs in the pressure measurement system. In total, 48 cases were evaluated through 166 runs, with a minimum of 3 runs per case. Experimental value variation within each case is represented as error bars in the figures below; to improve readability, variations of <5% are not depicted.

The butterfly valve used for measuring the external solids circulation consists of an air plenum and a porous plate, which enables fluidisation of the build-up of externally circulating solids when the valve is closed, as exemplified in Fig. 3a. With this set-up, the external circulation rate of solids was calculated from the increase rate of pressure in the plenum of the valve, when it was closed. The

velocity was adjusted to be maintained at 12·u_{mf} during the time when valve was closed. As shown in Fig. 3b, the valve plenum pressure increases linearly during a certain time interval, the length of which depends on the operating conditions. The higher the external solids flow, the shorter the time for which the valve can be closed without removing too much solids from the riser, to ensure that the measured values are not affected (typically 12%–36% of the original riser solids are removed to the return leg during the measurements). The external solids circulation is measured a minimum of three times for each case. In-between these measurements, the valve is re-opened and the system is operated for 2 min, to allow stable conditions.

From the pressure drop measurements above the primary air distributor, we identify three bottom region categories (Table 2).

- Category 1. The presence of a dense bed requires a minimum of three pressure measurements within the dense bed (Svensson et al., 1996), so as to confirm a straight line corresponding to a constant solids concentration with height. However, since the three lowest pressure taps are located at 0.1, 0.21, and 0.52 m above the air distributor, only dense beds that are taller than the latter height can be detected with full certainty. Note that a typical dense bed height for CFB boilers is reported in literature as being 0.4–0.6 m, and it decreases with fluidisation velocity (Svensson et al., 1996).

The two other categories in Table 2 are defined for the runs in which the pressure drop across the height interval covered by the three lowest pressure taps (0.1–0.52 m) is not linear, i.e., the presence of a dense bed cannot be confirmed.

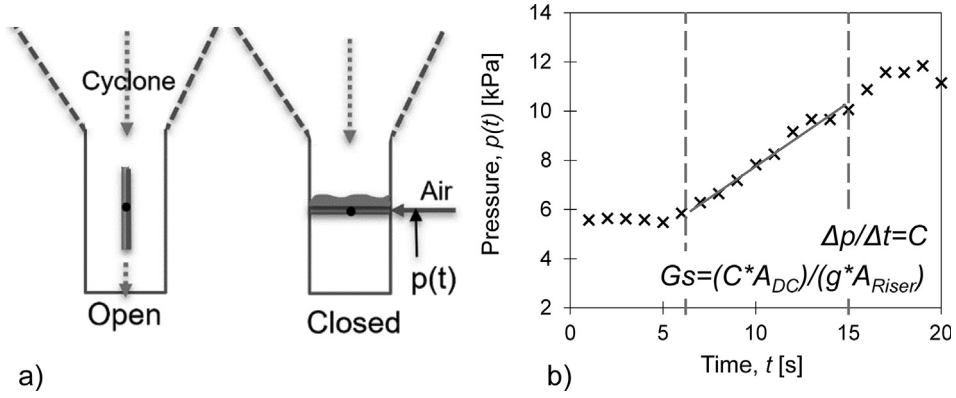

Fig. 3. a) Butterfly valve distributor used for measuring external circulation of solids. b) Pressure transient used to calculate the external circulation of solids.

Table 2
Criteria used to categorise the experimental runs as a function of the fluid-dynamics of the bottom-bed solids.

Category	Presence of a dense bed	*Symbol*		*Criterion 1:* Linear pressure drop across three measurements in bottom	*Criterion 2:* Bubble fraction < 0.5
1.	yes	■	Filled	yes	yes
2.	unclear	▬	Half-filled	no	yes
3.	no	□	Empty	no	no

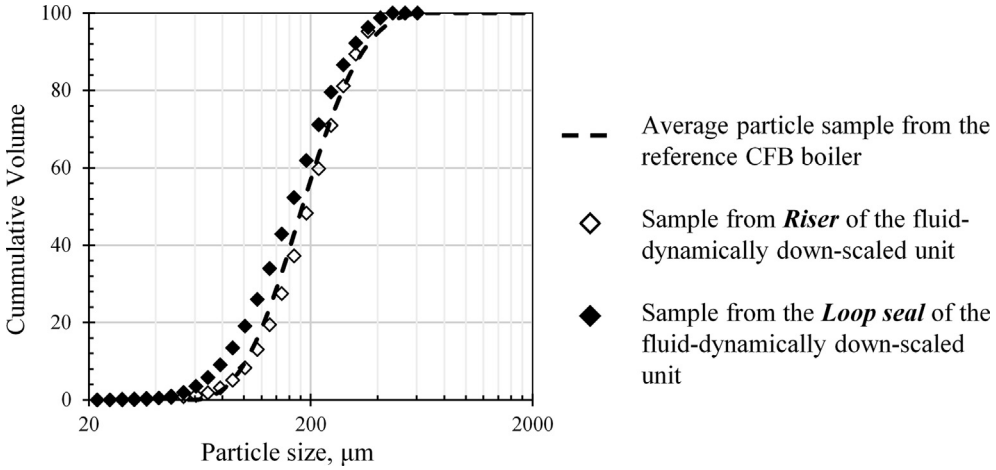

Fig. 4. Particle size distributions in the reference boiler and the fluid-dynamically down-scaled unit.

Table 3
Gas flows used for the validation cases.

		u_0 [m/s]$_{bottom}$	u_{top} [m/s]$_{top}$	u_{L2} [m/s]$_{top}$	u_{L1} [m/s]$_{top}$
Case 1	*Reference boiler*	3.00	3.47	0.35	1.28
	Fluid-dynamically down-scaled unit	3.15	3.41	0.31	1.17
Case 2	*Reference boiler*	2.35	2.67	1.04	0.19
	Fluid-dynamically down-scaled unit	2.31	2.46	0.89	0.16
Case 3	*Reference boiler*	1.96	2.17	0.79	0.19
	Fluid-dynamically down-scaled unit	1.88	2.04	0.71	0.18
Case 4	*Reference boiler*	1.46	1.49	0.41	0.18
	Fluid-dynamically down-scaled unit	1.86	1.65	0.33	0.18

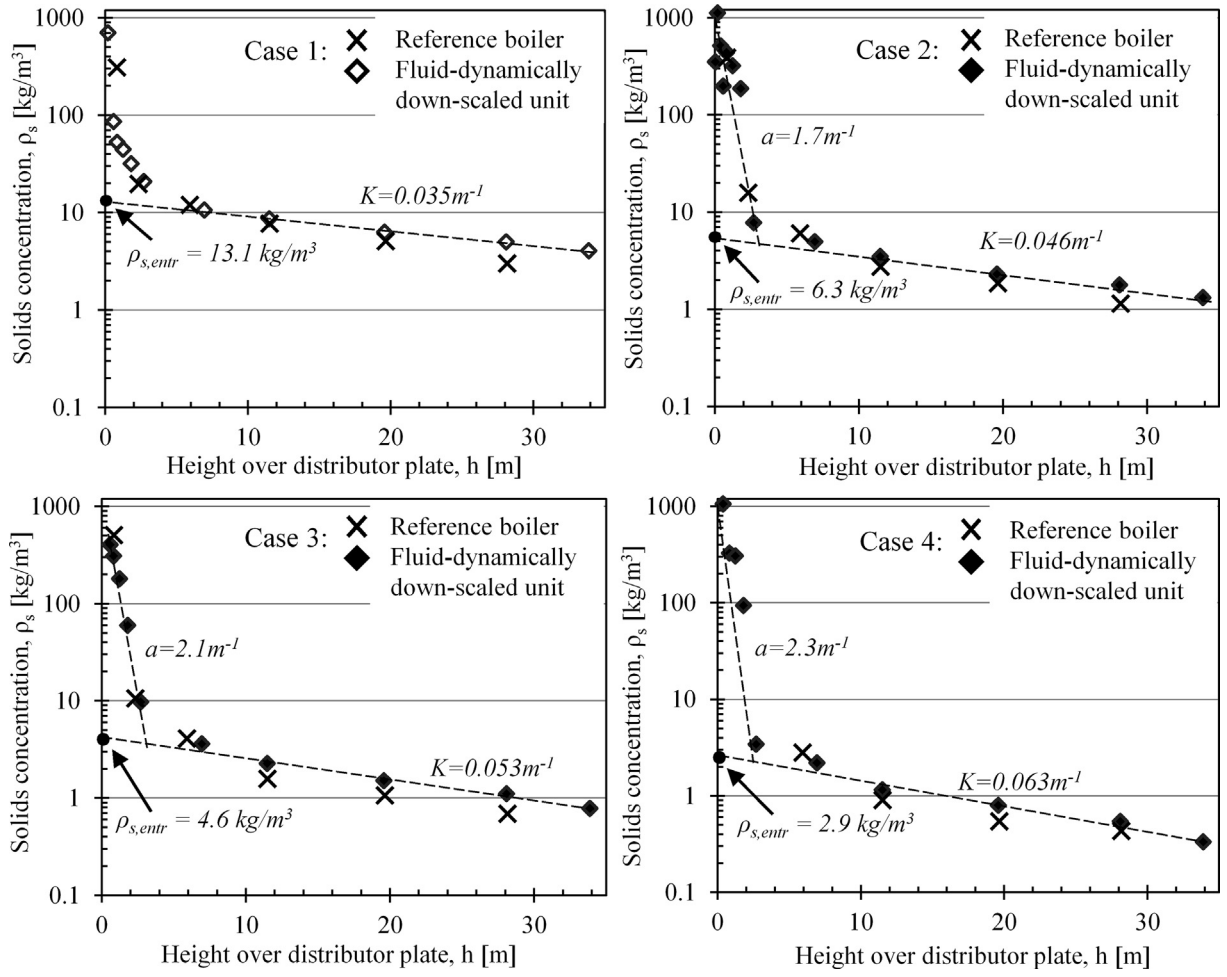

Fig. 5. Vertical profiles of solids concentrations measured in the 200-MW_{th} reference boiler and in the fluid-dynamically down-scaled unit for the cases given in Table 3.

- Category 2. The emulsion phase dominates, i.e., the emulsion phase occupies a larger volume than the bubble phase in the region located between the two lowest pressure taps. This is based on the assumption that the emulsion phase remains at the minimum level of fluidisation, which yields a threshold value for the solids concentration of 750 kg/m^3, above which the emulsion phase predominates.
- Category 3. A dense bed is likely to be absent, i.e., neither a linear pressure drop nor a dominant emulsion phase can be observed.

The symbols listed in Table 2 are used in this paper to indicate which of the above-mentioned categories the bottom region belongs to with respect to the above categories: Category 1 (filled symbols), Category 2 (half-filled symbols) or Category 3 (empty symbols).

3.4. Validation

As mentioned in Section 3.1, solids sampled in the loop seal of the reference boiler showed a median size of $d_{p,boiler}^{50}$ = 190 μm. The PSD of this solids sample is compared to that of the solids in the fluid-dynamically down-scaled unit (Fig. 4) that were sampled after the unit had been de-fluidised once the solids inventory had stabilised, i.e., the solids loss in the cyclone was negligible. Thus, the solids sampling gave mean sizes of the copper solids in the loop seal and the riser (when up-scaled) of 163 μm and 195 μm, respectively. This indicates a slight size-segregation effect and a mass-weighted value of 186 μm for the whole system, as compared to 175 μm for the fresh material.

The fluid-dynamically down-scaled unit is validated by means of the measured vertical profiles of the solids concentrations in

Table 4
Test matrix.

	Number of investigated cases	Primary air, u_0 (m/s)	Secondary air u_{2nd} (m/s)	ΔP_{riser} ranges (kPa)
Primary air only runs	**36** (130 runs, with at least 3 runs per case)	0.6–4.5	–	3.2–4.4 5.2–6.4 7.2–8.4
Secondary air runs	**12** (36 runs, with at least 3 runs per case)	1.4, 2.2, and 3.2	$u_{L.1}$ = 0.6 $u_{L.1}$ = 1.05 $u_{L.2}$ = 0.7 $u_{L.2}$ = 1.25	2.9–5.6

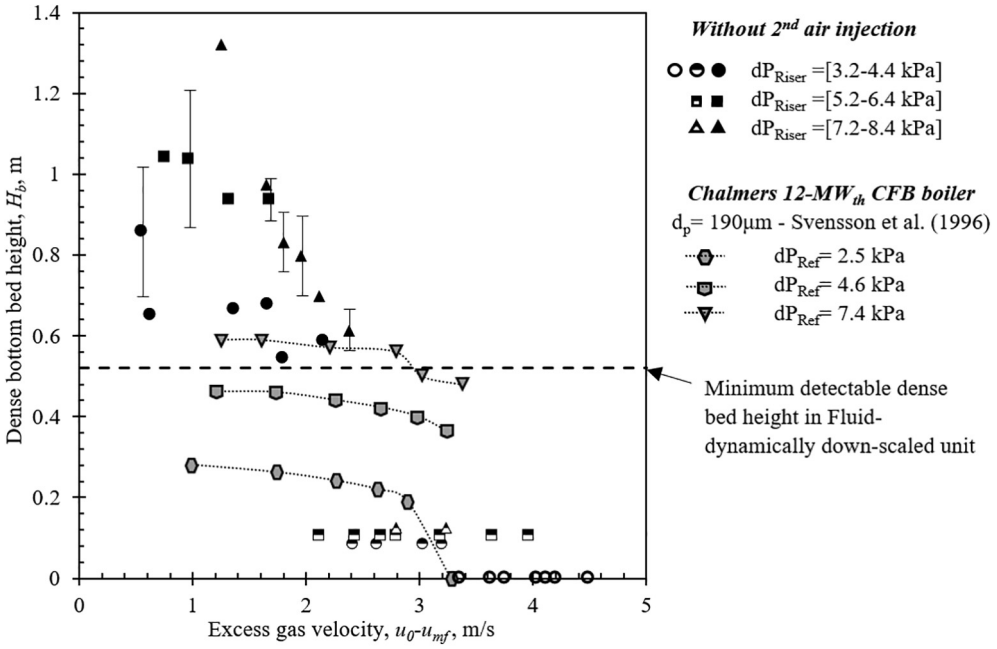

Fig. 6. Dense bed height as a function of excess gas velocity, as obtained from the measurements made in the down-scaled unit (representing a 200-MW_{th} CFB boiler) and the 12-MW_{th} Chalmers boiler (Svensson et al., 1996). Data from the down-scaled unit follow the symbols given in Table 2. Results from the Chalmers boiler are all plotted as grey symbols, even when H_b = 0.

the four different reference cases listed in Table 3. For these runs, a bottom section with tapered walls was used in the cold flow model. While the primary air velocity, u_0, is based on the cross-sectional area at the air distributor (i.e. at the bottom of the riser), the other superficial gas velocities in Table 3, u_{top}, $u_{L.1}$ and $u_{L.2}$, are related to the cross-sectional area above the tapered section in the riser (where $u_{L.1}$ and $u_{L.2}$ describe the corresponding contributions of the gas lateral injections at two heights). Thus, the total top velocity u_{top}, includes both primary air and the lateral air injection flows given (*cf.* Table 3).

Fig. 5 gives the vertical solids concentration profiles for the validation cases, both for the reference boiler and the fluid-dynamically down-scaled unit. It is clear that there is generally good agreement between the fluid-dynamically down-scaled unit and the reference boiler in all four cases. For Case 1, no dense bed height could be detected in the down-scaled unit, and the bubble fraction is slightly < 50%, resulting in the absence of a dense bed. This could not be investigated in the reference boiler due to a scarcity of pressure ports in the bottom region. For Cases 2–4, there is a dense bed in the bottom of the fluid-dynamically down-scaled unit (following the categorisation suggested in this work; Table 2).

3.5. Test matrix

Table 4 provides a summary of the test matrix used, together with the operational intervals for fluidisation velocity, gas lateral injections and riser pressure drop (measured between the bottom pressure tap at h = 0.1 m and the top of the riser). As mentioned above, these measurements applied a bottom section with vertical walls, so as to simplify the analysis by eliminating the bottom-effects caused by tapered walls.

4. Results and discussion

The results are presented below in an order that follows the solids flow, starting in the dense bottom bed and continuing towards the riser exit. The results from the scale model are presented as up-scaled values.

Most of the results are presented with the single-particle terminal velocity (u_t) of the solids in the riser. While this variable is known to vary somewhat from run to run, it was not possible to perform particle sampling and size distribution analysis for each run. Instead, these were carried out for a few runs and a general value of u_t = 1.06 m/s (corresponding to a particle size of 195 μm, from a sample in the riser) is assumed for all the cases presented below.

4.1. Flow regime in the bottom region

Fig. 6 shows the decrease in dense bed height with excess gas velocity, comparing the present measurements made in the scale model with literature data for the Chalmers 12-MW_{th} boiler with a mean solids size of 190 μm (Svensson et al., 1996). Note that

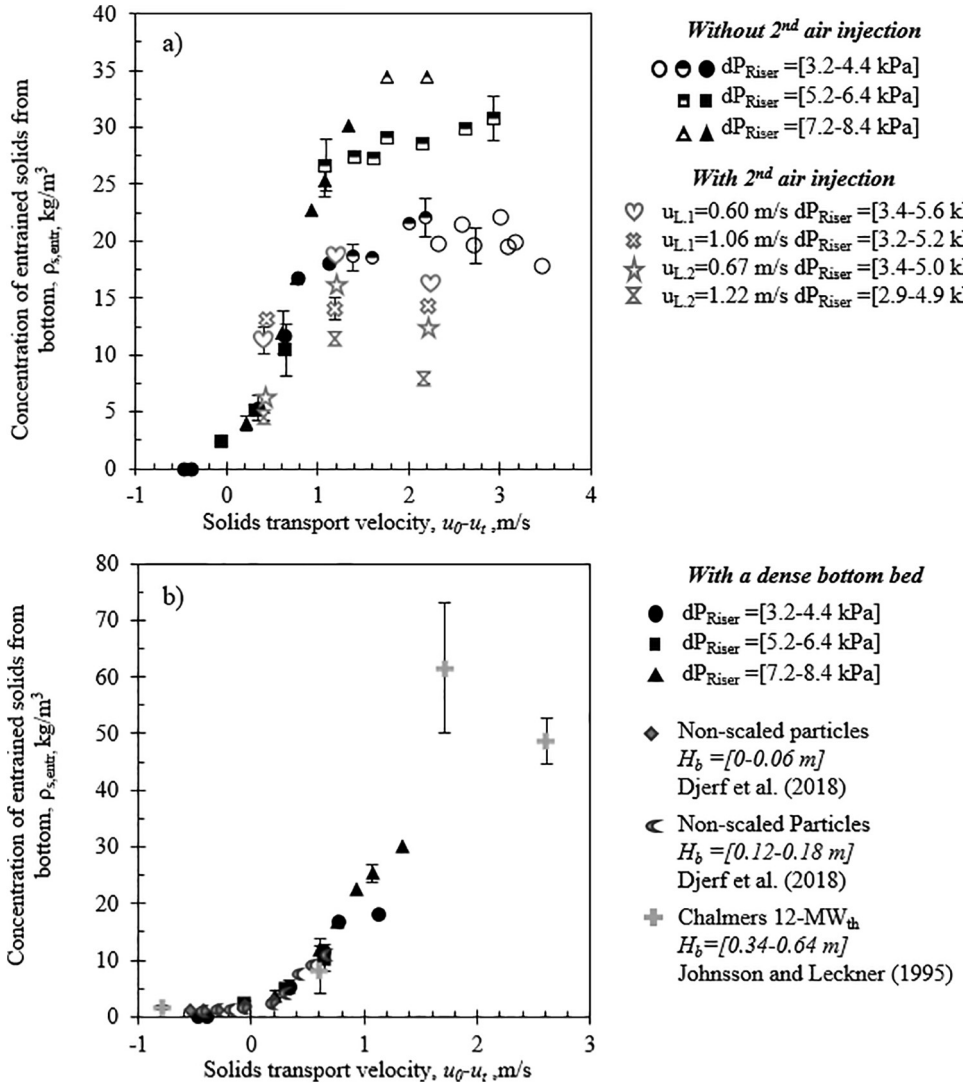

Fig. 7. Concentration of entrained solids from the bottom region as a function of the solids transport velocity for different riser pressure drops and bed heights, as obtained from the measurements made in the down-scaled unit (representing a 200-MW_{th} CFB boiler) and data from the literature. a) Results without and with secondary air injection. b) Concentration of entrained material with a confirmed dense bed from this study, non-scaled particles (Djerf et al., 2018), and the Chalmers 12-MW_{th} CFB boiler (Johnsson and Leckner, 1995).

for the scale model data are grouped in riser pressure drop intervals, while for the Chalmers boiler data each category implies a constant pressure drop over the bottom region (h = 0.1–1.6 m) only. It is evident that for a given pressure drop, the dense bed decreases in height with excess gas velocity and is eventually depleted. The cases run in the down-scaled unit with a low riser pressure drop cover all three categories of bottom region flow characteristics (*cf.* Table 2). Although none of the cases with the two higher riser pressure drop ranges result in depletion of the dense bottom bed, it is reasonable to assume that this would have been the case if the fluidisation velocity could have been increased further.

The results from the fluid-dynamically down-scaled unit indicate that, for riser pressure drops typically used in large-scale CFB boilers (7–8 kPa), the presence of a dense bottom bed is not obvious for excess gas velocities above 2.5 m/s. However, the Chalmers boiler data indicate that when the bottom riser pressure drop is maintained (by means of adding solids, as the fluidisation velocity increases) there is less of a decrease in the dense bed height with fluidisation velocity, although the dense bed is eventually depleted at 3.3 m/s for the lowest pressure drop series. Thus, it is likely that a dense bed cannot be maintained above a certain fluidisation velocity, which increases with furnace pressure drop. The presence or absence of a dense bed is an important aspect to know in the operation of CFB boilers, as it yields different bottom dynamics, which, as shown below, will influence the solids flow above the bottom region.

4.2. Entrainment of solids from the bottom region

Fig. 7 summarises the results for the solids entrainment from the bottom region, as indicated by the concentration of entrained solids from the bottom, $\rho_{s,entr}$ [see Eq. (1.3)], as a function of the single-particle transport velocity (u_0-u_t). As shown in Fig. 7a, the concentration of entrained solids increases with the solids transport velocity in the presence of a dense bed (Category 1; filled symbols). However, it becomes saturated as the dense bed is depleted (Categories 2 and 3; half-filled and empty symbols, respectively). The dense bed can be regarded as acting as a buffer for solids, in that if it is present it increases the concentration of entrained solids as the fluidisation velocity is increased. Since higher riser pressure drops maintain a

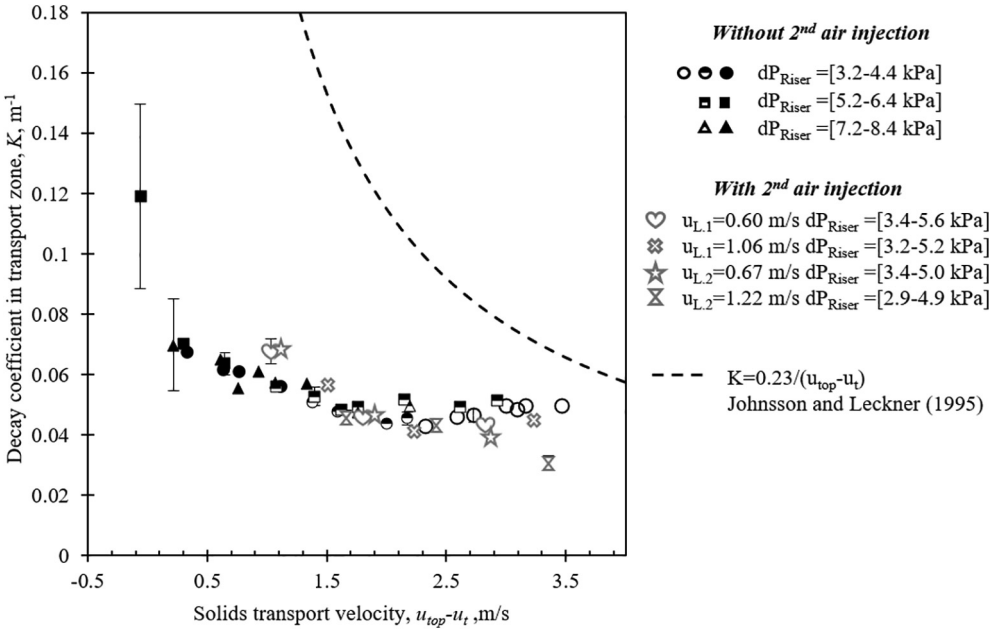

Fig. 8. Back-mixing from the core region to the wall layers, characterised by the decay coefficient, K, as a function of the solids transport velocity, as obtained from the measurements made in the down-scaled unit, representing a 200-MW_{th} CFB boiler. Secondary air cases are depicted by grey symbols and the correlation obtained in the Chalmers 12-MW_{th} CFB boiler (Johnsson and Leckner, 1995) is indicated by the dashed line.

dense bed at higher fluidisation velocities (see Fig. 6), higher pressure drops yield higher values for the concentration of entrained solids (Fig. 7a). Note that in presence of a dense bed, the riser pressure drop does not influence the concentration of entrained solids at a given fluidisation velocity. The data-points corresponding to the grey symbols in Fig. 7a represent the influence of the secondary air.

Fig. 7b compares the concentrations of entrained solids from the present measurements (resembling the 200-MW_{th} boiler) with data from the Chalmers 12-MW_{th}^{h} CFB boiler (Johnsson and Leckner, 1995) and from previous experimental work carried out by the authors in the same down-scaled unit operated with glass particles (Djerf et al., 2018). In order to remove the effect of depletion of the dense bed, only data for which a dense bed could be confirmed are included in Fig. 7b. The glass particle experiments did not apply the scaling proposed by Glicksman, but the scaling described by Van der Meer et al. (1999) can be applied in order to resemble hot conditions, yielding a length scale factor of 1/1.5, which should result in the cold flow model resembling a hot unit with a cross-section that is about half of that in the Chalmers boiler. Thus, the results in Fig. 7b can be seen as representing three different boilers with good agreement between the values for the Chalmers boiler, the present work (200-MW_{th} boiler), and the present unit operated with glass beads (resembling a small boiler). This indicates that the concentration of entrained solids is independent of boiler geometry.

Fig. 7a includes the results from runs that involved lateral injections of gas into the riser. It should be noted that the values for these specific runs are plotted against the solids transport velocity based on the primary air velocity, as the entrainment is assumed to occur at the level of the dense bed height (all other values which include the lateral air injection apply the total top velocity). In general, lateral gas injections yield a decreased concentration of entrained solids, presumably due to disturbance of the solids upflow causing less solids to be lifted, which is in line with previous works (Cho et al., 1994; Kalaga et al., 2020) in laboratory-scale units but not with the results from one run in the Chalmers boiler (Johnsson and Leckner, 1995). The only exceptions to this trend are the two cases in which the air was injected into the dense bottom bed, which resulted in an increase in the concentration of entrained solids. These two cases arise when the dense bottom bed is high, at a low fluidisation velocity and a high riser pressure drop, and at the low air injection point. Fig. 7a also shows the influence of gas injection height, whereby the higher location (L.2) yields a lower concentration of entrained solids compared to the lower location (L.1). In addition, Fig. 7a shows that higher secondary air flows generally yield lower concentrations of entrained solids. Thus, while air staging is an efficient primary measure to tackle emissions and control the load of large-scale CFB boilers, it can reduce the solids hold-up in the upper part of the riser and this may have a significant impact on the heat balance.

4.3. Back-mixing to the wall layers

Fig. 8 shows the exponential decay coefficient in the transport zone, *K* [see Eq. (1)], which expresses the back-mixing to the wall layers as a function of the solids transport velocity in the upper part of the riser. It is shown that back-mixing to the wall layers is influenced neither by the presence/absence of a dense bed nor by the riser pressure drop. This agrees with previous studies conducted by the authors without fluid-dynamical down-scaling (Karlsson et al., 2017; Djerf et al., 2018).

Fig. 8 shows that secondary air has little influence on the solids back-mixing to the wall layers (note that the solids transport velocity is based on the velocity above the secondary air inlets). Fig. 8 includes the correlation for *K* proposed previously (Johnsson and Leckner, 1995) based on measurements performed in the Chalmers 12-MW_{th} CFB boiler. Those previous results are significantly different from the results of the present work. A possible explanation for this discrepancy is that the scaling applied in the present work resembles a much larger (200-MW_{th}) boiler than the Chalmers boiler, yielding significantly less back-mixing to the walls, thereby revealing that the back-mixing mechanism depends on the size of the unit, as mentioned in Section 2.1.

4.4. Upward and external fluxes of solids

The solids flow in the top region of the riser involves an upward flux in the core domain, of which a share of the solids escapes the riser into the cyclone and forms the external circulation of solids, while the remainder is internally re-circulated by means of back-flow to the wall layers (Section 4.3).

Fig. 9 compares the calculated upward flux of solids at the riser top (Fig. 9a) and the measured external circulation of solids (Fig. 9b). There is an obvious increase in the upward solids flux at the riser top [calculated with Eq. (2)], as well as an increase in the external circulation of solids with an increase in the solids transport velocity, when a dense bed is present. With an increase in the solids transport velocity, the difference between the upward core flux and the measured external solids circulation increases, indicating a significant back-flow effect in the top of the riser. Thus, using the calculated upward core flux as a measure of the external solids segregation does not give a good approximation at higher velocities. Fig. 9a also shows (grey symbols) the effect of lateral gas injections, which in general terms are characterised by a reduction in the upward solids flux. The reduction in upward solids flux is based on the hindering effect of entrained solids from the bottom region and a minor influence of the back-mixing to the wall layer (in any direction, see Sections 4.2 and 4.3). Thus, the lateral gas injection leads to a lower upward flux of solids at the top of the riser. However, since there is no obvious effect on the external circulation of solids, this implies that the lateral gas injection reduces the back-flow ratio (see below).

Fig. 10 presents the values for the external circulation of solids, here measured in the return leg, as compared to the values in the literature (Werdermann, 1993; Johansson, 2005; Zhang et al., 1995; Edvardsson et al., 2006; Yue et al., 2005), as a function of the fluidisation velocity. Note that this figure contains data from units that differ significantly in size. Therefore, direct comparisons of the data are not intended, only qualitative comparisons. Most of the literature values are estimated as the upward core solids flux, as given by Eq. (2) (*cf.* Fig. 9a). Thus, the same pattern observed for Fig. 9, a and b is seen here: the solids circulation values from the literature, estimated from measurements in the riser (the light grey area of Fig. 10) are consistently higher than those calculated from local measurements in the return leg, i.e., in this work and that of Edvardsson et al. (2006), who estimated the external solids circulation from a heat balance over the loop seal (Edvardsson et al., 2006) (the dark grey area of Fig. 10).

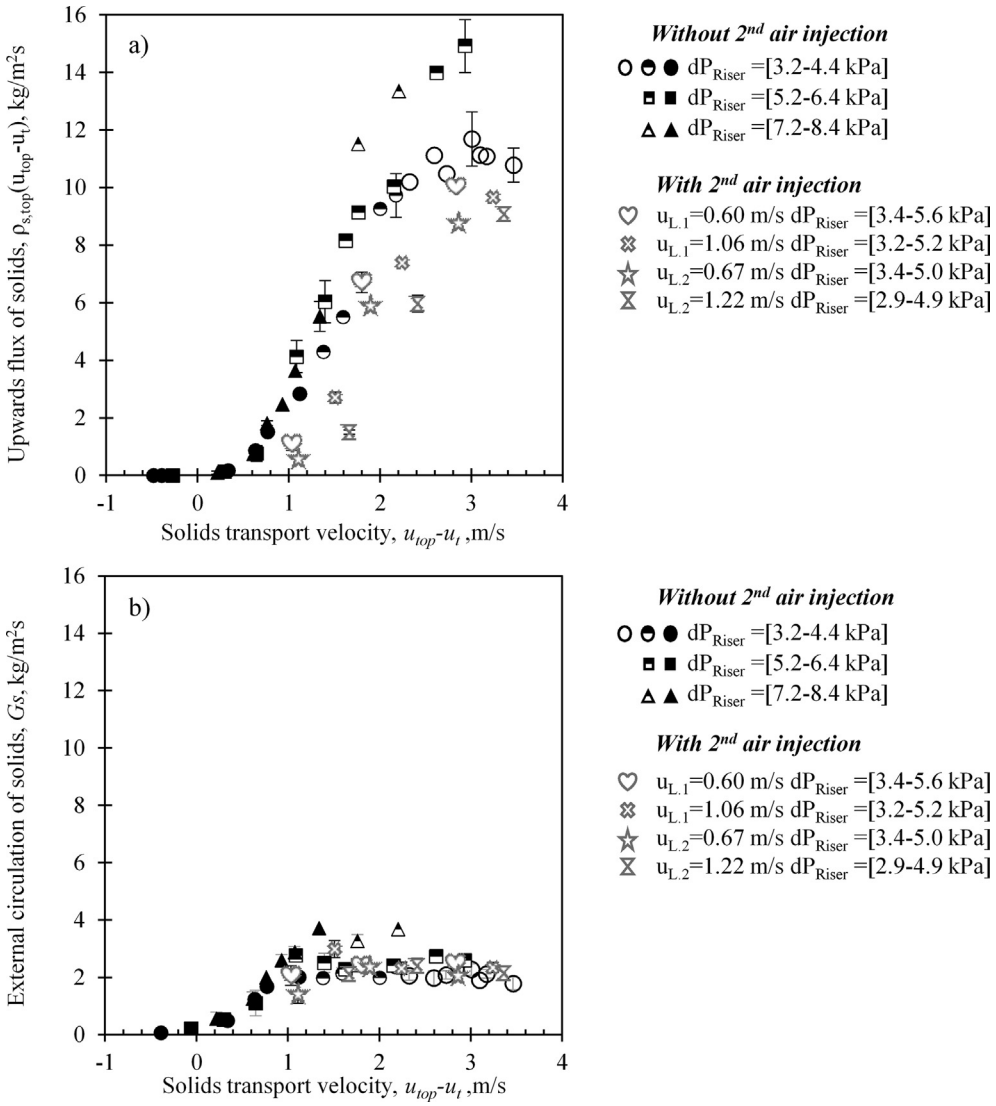

Fig. 9. Comparison of upward solids fluxes in the core region at the top of the riser, as obtained from the measurements carried out in the down-scaled unit, representing a 200-MW$_{th}$ CFB boiler (a), as obtained from Eq. (1) and the measured external circulation of solids (b), for runs with and without secondary air.

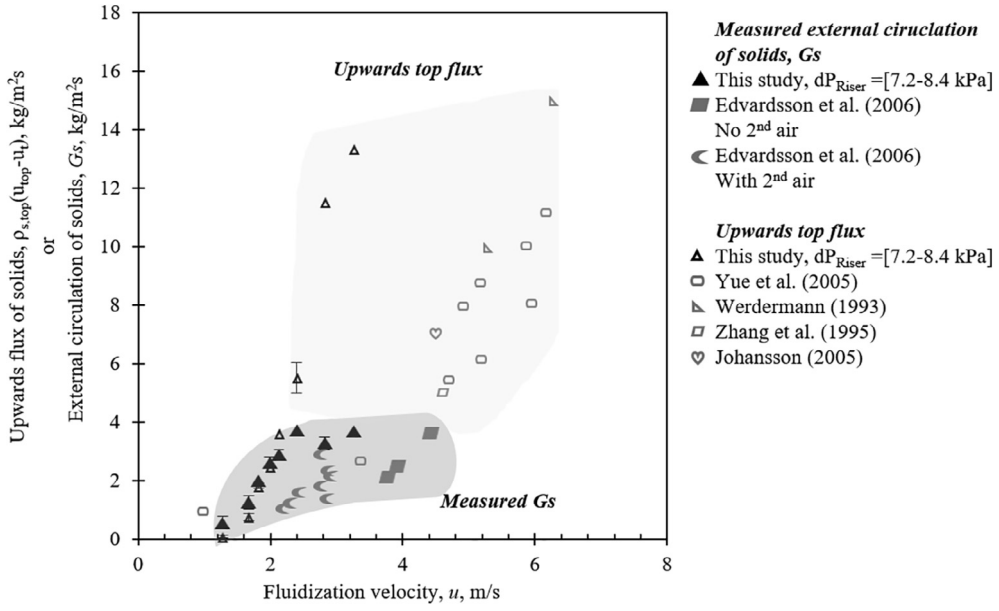

Fig. 10. External solids circulation. Present study measurements compared to literature values for large CFB boilers (Werdermann, 1993; Johansson, 2005; Zhang et al., 1995; Edvardsson et al., 2006; Yue et al., 2005).

4.5. Back-flow ratio

Fig. 11a compares the measured external circulation of solids to the corresponding estimated solids upwards flux at the top of the riser, i.e., the deviation from the diagonal line represents the solids back-flow. At low fluidisation velocities (i.e., low values of the solids upward flux), all the solids reaching the riser top are externally circulated, i.e., the back-flow is negligible ($k_b \sim 0$), while the back-flow becomes dominant at higher values of the upwards flux of solids (in agreement with previous reports (Pallares and Johnsson, 2006), with values of k_b up to 0.8, meaning that 80% of the upward flux of solids in the top of the riser (*cf.* Fig. 9a) are internally re-circulated. It should be noted that since particle size segregation along the riser is likely, the solids size at the top of the riser needs to be accounted for when estimating the upward flux of solids, so as to avoid negative back-flow values. However, such sampling is complicated, and it also changes with the operating conditions. In this study, the particle sample from the solids in the riser was used for the estimation of the terminal velocity (*cf.* Section 4), therefore, also for the upward flux of solids, possibly leading to an overestimation of the terminal velocity, especially for cases with low fluidisation velocities.

By comparing the estimations of the external circulation of solids in the Chalmers 12-MW$_{th}$ CFB boiler made by Edvardsson et al. (2006) with the upward solids flux calculated from measurements conducted by Johnsson and Leckner (1995) under similar operational conditions, the back-flow is estimated to be within the range of 0.83–0.89. Based on the literature (Werdermann, 1993; Werther, 1993), Werther (1993) estimated the back-flow in a 109-MW$_{th}$ CFB boiler to be 0.2, through comparison of the upwards and downwards solids fluxes in the top of the furnace. It should be borne in mind that the geometry of the exit configuration in the fluid-dynamically down-scaled unit used for the tests reported in the present work had a flat roof and, thus, did not correspond to the geometry of the inclined roof in the reference boiler. Yet, the influence of the geometry at the top of the riser/furnace has been reported to have only a small impact on the back-flow under flow conditions relevant for CFB boilers (Van der Meer et al., 2000). Nevertheless, this effect is relevant, as the value of k_b increased from 0 to 0.4 when a smooth exit was replaced by an abrupt one (Werther, 1993).

Some studies in the literature have reported an influence of the fluidisation velocity in the loop seal on the external circulation of solids (Bidwe et al., 2011; Han et al., 2007; Cheng and Basu, 1999; Basu and Cheng, 2000). However, the units used in those studies were small and had a return leg configuration, which differs from that in large-scale CFB boilers; in the latter, the return leg is designed with wide geometries and operated under well-above-minimum fluidisation conditions, thus turning the riser - rather than the return system – into the loop element governing the net circulation of solids (Johansson et al., 2006; Li et al., 2018; Wang et al., 2014). In order to rule out the possibility that the seal fluidisation acts as a limiter of the solids net flow, three runs were carried out in which only the fluidisation velocity in the loop seal was varied (plotted with grey markings in Fig. 11a). It is clear that there are no significant differences in the external solids circulation between these runs, and, therefore, no differences in the back-flow.

Since the solids back-flow originates from the inability of solids to follow the gas as it bends into the exit duct to the cyclone, the Stokes number (describing the extent to which particles are unable to follow a fluid) should be governing this phenomenon. Fig. 11b shows the back-flow ratios for different Stokes numbers with the characteristic length in the Stokes number taken as half of the depth of the unit, which should be a reasonable assumption for representing the bend experienced by the gas flow at the exit region. However, the St-number would only allow for comparisons of different sizes of similar exit configurations, but can hardly be expected to be useful for comparing different geometries (smooth, abrupt, exit window size and geometry, etc). In this sense, the change in backflow with St-number is to be assigned to the particular geometry investigated, rather than be used as a general value. As shown in Fig. 11b, the back-flow is almost non-existent at low Stokes numbers, there is a transition for Stokes numbers in the range of 0.08–0.12 as the back-flow increases rapidly, and thereafter it levels of at Stokes numbers > 0.12. Theoretically, with a further increase in velocity (and in Stokes number) the back-flow ratio would approach a value of 1, as the gas drag would not be able to overcome the high inertia of the solids (the drag on the solids is constant, since the slip velocity between the gas and solids remains equal to the terminal velocity of the particles). However, the fan capacity limits investigations at higher velocities than

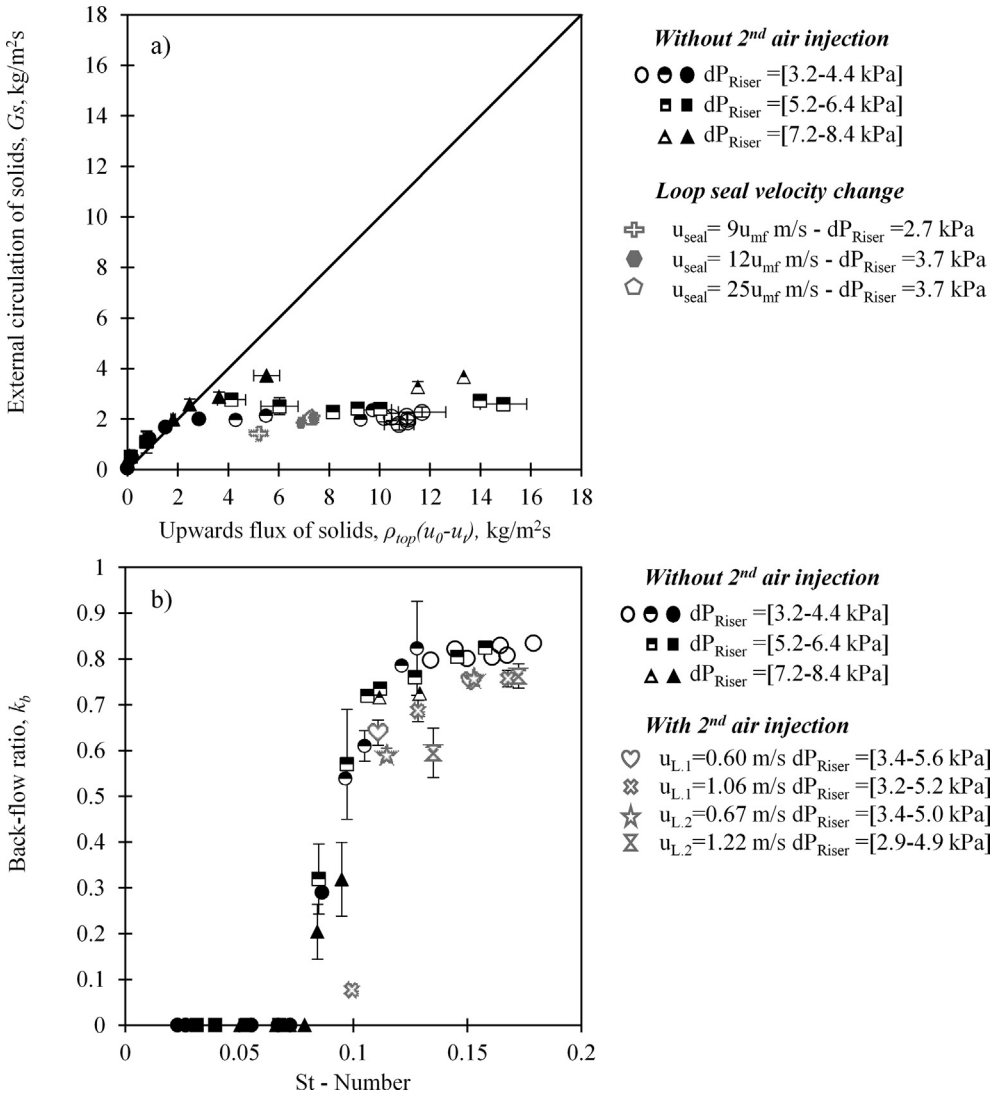

Fig. 11. Back-flow effect. a) Measured external solids circulation compared to estimate the upwards flux of solids at the top of the riser. b) Back-flow ratio as a function of the Stokes number. From the measurements in the down-scaled unit, representing a 200-MW_{th} CFB boiler.

Table 5
Solids sizes in the down-scaled unit, as obtained from the measurements made in the down-scaled unit (up-scaled values), representing a 200-MW_{th} CFB boiler.

Sample	d_{p10} (μm)	d_{p50} (μm)	d_{p90} (μm)	$u_t(d_{p10})$ (m/s)	$u_t(d_{p50})$ (m/s)	$u_t(d_{p90})$ (m/s)
Riser	106	**195**	323	0.35	**1.06**	2.45
Loop seal u_0 = 1.7 m/s	69	130	238	0.15	0.50	1.48
Loop seal u_0 = 2.7 m/s	78	158	299	0.19	0.72	2.16
Loop seal u_0 = 3.6 m/s	81	163	301	0.20	0.77	2.20
Filter sample	48	111	251	0.07	0.38	1.63

those shown in this study. Fig. 11b also shows that the secondary air injections lower only somewhat the back-flow ratio.

4.6. Size segregation

Table 5 shows the measured solids size segregation patterns in terms of the differences between samples from the riser and the loop seal (sampled after de-fluidisation), together with the corresponding values for the terminal velocity.

The table shows the segregation effect, as the particle size in the loop seal is lower than in the riser. This is a consequence of size segregation being present in all the mechanisms discussed above (solids entrainment from the bottom, back-mixing to the wall layers and back-flow at the riser exit), as shown by the results of the present work. As expected, the solids size in the loop seal increases

with an increase in fluidisation velocity, as the probability of entraining coarser particles from the bottom region into the upwards core flow increases with fluidisation velocity.

5. Conclusions

A fluid-dynamically down-scaled unit resembling an existing 200-MW_{th} utility CFB boiler was built and operated according to the simplified scaling laws proposed by Glicksman et al. (1993). A comparison of samples of in-furnace solids acquired from the two units shows that the down-scaled model is operated with solids that have a size distribution similar to that of the full-scale boiler. The pressure drop profiles (concentration profiles) measured in the scale model show good agreement with the corresponding measurements obtained in the 200-MW_{th} CFB boiler.

The results from an experimental campaign that covered a broad range of operational parameters were used to elucidate the mechanisms governing the solids flow pattern in CFB furnaces. The results show that the presence or absence of a dense bed governs the entrainment of solids from the bottom region, which increases with the fluidisation velocity as long as a dense bed is maintained. However, when the dense bed is depleted the solids entrainment becomes saturated. Lateral injections of air from the riser walls into the freeboard (secondary air) hinder the solids entrainment, whereas injection of air into the dense bed enhances entrainment of the solids.

The back-mixing to the wall layer is shown – in line with the previous literature - to be dependent upon the fluidisation velocity and the cross-sectional dimensions.

The solids back-flow at the exit region goes from being negligible at low Stokes numbers (i.e., low gas velocities) to gradually approaching unity for higher Stokes numbers. Thus, it is shown that the external solids flux should not be estimated from pressure drop measurements at the top of the furnace (i.e., from estimating the upward solids flux by multiplying the top solids concentration by an estimated solids transport velocity).

CRediT authorship contribution statement

Tove Djerf: Investigation, Formal analysis, Writing. **David Pallarès:** Supervision, Writing. **Filip Johnsson:** Supervision, Writing.

Declaration of Competing Interest

The authors declare that they have no known competing financial interests or personal relationships that could have appeared to influence the work reported in this paper.

Acknowledgements

The authors acknowledge financial support from the Swedish Energy Agency within the framework of project 38347-2, and from the boiler manufacturer Valmet Technologies Oy.

The authors also acknowledge the modelling work on the design of the cyclone for the fluidised down-scale unit conducted by Dr. Ulrich Muschelknautz at MK Engineering.

References

Basu, P., Cheng, L., 2000. An analysis of loop seal operations in a circulating fluidized bed. Chem. Eng. Res. Des. 78 (7), 991–998.

Bidwe, A., Chariots, A., Dieter, H., Wei, A., Zieba, M., Scheffknecht, G., 2011. A study of standpipe and loop seal behavior in circulating fluidized bed for Geldart B particles. In: Proceedings of the 10th international conference on circulating fluidized beds combustion. 2011. Citeseer.

Cai, R., Zhang, H., Zhang, M., Yang, H., Lyu, J., Yue, G., 2018. Development and application of the design principle of fluidization state specification in CFB coal combustion. Fuel Process. Technol. 174, 41–52.

Cheng, L., Basu, P., 1999. Effect of pressure on loop seal operation for a pressurized circulating fluidized bed. Powder Technol. 103 (3), 203–211.

Cho, Y.J., Namkung, W., Kim, S.D., Park, S., 1994. Effect of secondary air injection on axial solid holdup distribution in a circulating fluidized bed. J. Chem. Eng. Jpn. 27 (2), 158–164.

Couturier, M., Doucette, B., Stevens, D., Poolpol, S., Razbin, V., 1991. Temperature, gas concentration and solid mass flux profiles within a large circulating fluidized bed combustor. In: 11th International Conference on FBC, ASME. 1991. Montreal.

Davidson, J., 2000. Circulating fluidised bed hydrodynamics. Powder Technol. 113 (3), 249–260.

Djerf, T., Pallarès, D., Johnsson, F., 2018. Bottom-bed fluid dynamics–Influence on solids entrainment. Fuel Process. Technol. 173, 112–118.

Edvardsson, E., Åmand, L.-E., Thunman, H., Leckner, B., Johnsson, F.2006. Measuring the external solids flux in a CFB boiler. In: Proceedings of the 19th FBC Conferance. 2006. Vienna Austria.

Glicksman, L.R., 1984. Scaling relationships for fluidized beds. Chem. Eng. Sci. 39 (9), 1373–1379.

Glicksman, L., Hyre, M., Woloshun, K., 1993. Simplified scaling relationships for fluidized beds. Powder Technol. 77 (2), 177–199.

Glicksman, L., Hyre, M., Farrell, P., 1994. Dynamic similarity in fluidization. Int. J. Multiph. Flow 20, 331–386.

Gómez-Barea, A., Leckner, B., 2010. Modeling of biomass gasification in fluidized bed. Prog. Energy Combust. Sci. 36 (4), 444–509.

Han, X., Cui, Z., Jiang, X., Liu, J., 2007. Regulating characteristics of loop seal in a 65 t/h oil shale-fired circulating fluidized bed boiler. Powder Technol. 178 (2), 114–118.

Hannes, J.P., 1998. Mathematical modelling of circulating fluidized bed combustion.

Horio, M., Ishii, H., Kobukai, Y., Yamanishi, N., 1989. A scaling law for circulating fluidized beds. J. Chem. Eng. Jpn. 22 (6), 587–592.

Huttunen, M., Peltola, J., Kallio, S., Karvonen, L., Niemi, T., Ylä-Outinen, V., 2017. Analysis of the processes in fluidized bed boiler furnaces during load changes. Energy Procedia 120, 580–587.

Johansson, A., Johnsson, F., Andersson, B.-Å., 2006. The performance of a loop seal in a CFB boiler. J. Energy Res. Technol. 128 (2), 135–142.

Johansson, A., Johnsson, F., Leckner, B., 2007. Solids back-mixing in CFB boilers. Chem. Eng. Sci. 62 (1–2), 561–573.

Johansson, A., 2005. Solids flow pattern in circulating fluidized-bed boilers.

Johnsson, F., Leckner, B.. Vertical distribution of solids in a CFB-furnace. In: CONF-950522. 1995. American Society of Mechanical Engineers, New York, NY (United States).

Johnsson, F., Andersson, S., Leckner, B., 1991. Expansion of a freely bubbling fluidized bed. Powder Technol. 68 (2), 117–123.

Johnsson, F., Zhang, W., Leckner, B. Characteristics of the formation of particle wall-layers in CFB boilers. In: Proceedings of the second international conference on multiphase flow. 1995. The Japan Society of Multiphase Flow Nagoya.

Johnsson, F., Leckner, B., Vrager, A., 1999. Solids flow pattern in the exit region of a CFB–Furnace influence of exit geometry. In: CONF-990534. 1999. Chalmers Univ. of Technology, Göteborg (SE).

Kalaga, D.V., Ansari, M., Turney, D.E., Hernandez-Alvarado, F., Kleinbart, S., ArunKumar, K., Joshi, J.B., Banerjee, S., Kawaji, M., 2020. Scale-up of a downflow bubble column: experimental investigations. Chem. Eng. J. 386, 121447.

Karlsson, T., Liu, X., Pallarès, D., Johnsson, F., 2017. Solids circulation in circulating fluidized beds with low riser aspect ratio and varying total solids inventory. Powder Technol. 316, 670–676.

Koornneef, J., Junginger, M., Faaij, A., 2007. Development of fluidized bed combustion—an overview of trends, performance and cost. Prog. Energy Combust. Sci. 33 (1), 19–55.

Kunii, D., Levenspiel, O., 1991. Fluidization engineering. 1991.

Kunii, D., Levenspiel, O., 1990. Entrainment of solids from fluidized beds I. Hold-up of solids in the freeboard II. Operation of fast fluidized beds. Powder Technol. 61 (2), 193–206.

Lafanechere, L., Jestin, L., 1995. Study of a circulating fluidized bed furnace behavior in order to scale it up to 600 MWe. 1995, American Society of Mechanical Engineers, New York, NY (United States).

Leckner, B., 1998. Fluidized bed combustion: mixing and pollutant limitation. Prog. Energy Combust. Sci. 24 (1), 31–61.

Leckner, B., 2017. Regimes of large-scale fluidized beds for solid fuel conversion. Powder Technol. 308, 362–367.

Leckner, B., Szentannai, P., Winter, F., 2011. Scale-up of fluidized-bed combustion – a review. Fuel 90 (10), 2951–2964.

Leretaille, P., Werther, J., Briand, P., Montat, D., 1999. Modeling of hydrodynamics of large scale atmospheric circulating fluidized bed coal combustors. 1999, Technical Univ. Hamburg-Harburg, Hamburg (DE).

Li, C., Zou, Z., Li, H., Zhu, Q., 2018. A hydrodynamic model of loop seal with a fluidized standpipe for a circulating fluidized bed. Particuology 36, 50–58.

Löffler, G., Kaiser, S., Bosch, K., Hofbauer, H., 2003. Hydrodynamics of a dual fluidized-bed gasifier—Part I: simulation of a riser with gas injection and diffuser. Chem. Eng. Sci. 58 (18), 4197–4213.

Markström, P., Lyngfelt, A., 2012. Designing and operating a cold-flow model of a 100 kW chemical-looping combustor. Powder Technol. 222, 182–192.

Minchener, A., 2003. Fluidized bed combustion systems for power generation and other industrial applications. Proc. Inst. Mech. Eng. A: J. Power Energy 217 (1), 9–18.

Mirek, P., 2016. Influence of the model scale on hydrodynamic scaling in CFB Boilers. Braz. J. Chem. Eng. 33 (4), 885–896.

Myöhänen, K., 2011. Modelling of combustion and sorbent reactions in three-dimensional flow environment of a circulating fluidized bed furnace. Acta Universitatis Lappeenrantaensis.

Pallares, D., Johnsson, F., 2006. Macroscopic modelling of fluid dynamics in large-scale circulating fluidized beds. Prog. Energy Combust. Sci. 32 (5–6), 539–569.

Pallarès, D., 2008. Fluidized Bed Combustion: Modeling and Mixing. 2008, Chalmers University of Technology.

Sasic, S., Johnsson, F., Leckner, B., 2004. Interaction between a fluidized bed and its air-supply system: some observations. Ind. Eng. Chem. Res. 43 (18), 5730–5737.

Sasic, S., Leckner, B., Johnsson, F., 2007. Characterization of fluid dynamics of fluidized beds by analysis of pressure fluctuations. Prog. Energy Combust. Sci. 33 (5), 453–496.

Schöny, G., Zehetner, E., Fuchs, J., Pröll, T., Sprachmann, G., Hofbauer, H., 2016. Design of a bench scale unit for continuous CO2 capture via temperature swing adsorption—fluid-dynamic feasibility study. Chem. Eng. Res. Des. 106, 155–167.

Schouten, J.C., Zijerveld, R.C., van den Bleek, C.M., 1999. Scale-up of bottom-bed dynamics and axial solids-distribution in circulating fluidized beds of Geldart-B particles. Chem. Eng. Sci. 54 (13–14), 2103–2112.

Senior, R.C., Brereton, C., 1992. Modelling of circulating fluidised-bed solids flow and distribution. Chem. Eng. Sci. 47 (2), 281–296.

Sette, E., Pallarès, D., Johnsson, F., 2014. Experimental quantification of lateral mixing of fuels in fluid-dynamically down-scaled bubbling fluidized beds. Appl. Energy 136, 671–681.

Svensson, A., Johnsson, F., Leckner, B., 1996. Bottom bed regimes in a circulating fluidized bed boiler. Int. J. Multiph. Flow 22 (6), 1187–1204.

Svensson, A., Johnsson, F., Leckner, B., 1996. Fluidization regimes in non-slugging fluidized beds: the influence of pressure drop across the air distributor. Powder Technol. 86 (3), 299–312.

Van der Meer, E., Thorpe, R., Davidson, J., 1999. Dimensionless groups for practicable similarity of circulating fluidised beds. Chem. Eng. Sci. 54 (22), 5369–5376.

Van der Meer, E., Thorpe, R., Davidson, J., 2000. Flow patterns in the square cross-section riser of a circulating fluidised bed and the effect of riser exit design. Chem. Eng. Sci. 55 (19), 4079–4099.

Wang, P., Yao, X., Yang, H., Zhang, M., 2014. Impact of particle properties on gas solid flow in the whole circulating fluidized bed system. Powder Technol. 267, 193–200.

Wen, C., Chen, L., 1982. Fluidized bed freeboard phenomena: entrainment and elutriation. AIChE J. 28 (1), 117–128.

Werdermann, C.C., Feststoffbewegung und Wärmeübergang in zirkulierenden Wirbelschichten von Kohlekraftwerken. 1993: Shaker.

Werther, J., 1993 Fluid mechanics of large-scale CFB units. In: Proceedings of 4th International CFB Conference.

Wischnewski, R., Ratschow, L., Hartge, E.-U., Werther, J., 2010. Reactive gas–solids flows in large volumes—3D modeling of industrial circulating fluidized bed combustors. Particuology 8 (1), 67–77.

Xu, J., Lu, X., Wang, Q., Dong, Y., Wang, H., Chen, Y., Li, X., Lei, X., Zhang, W., Chen, J., 2015. Experimental study on gas-solid flow characteristics in a 60-meter-high CFB cold test apparatus. In: Proceedings of the 22nd International Conference on Fluidized Bed Conversion. 2015. Turku, Finland.

Yang, H., Yue, G., Xiao, X., Lu, J., Liu, Q., 2005. 1D modeling on the material balance in CFB boiler. Chem. Eng. Sci. 60 (20), 5603–5611.

Yang, H., Zhang, H., Yang, S., Yue, G., Su, J., Fu, Z., 2009. Effect of bed pressure drop on performance of a CFB boiler. Energy Fuels 23 (6), 2886–2890.

Yue, G., Lu, J., Zhang, H., Yang, H., Zhang, J., Liu, Q., Li, Z., Joos, E., Jaud, P., 2005. Design theory of circulating fluidized bed boilers. In: 18th International Conference on Fluidized Bed Combustion. 2005. American Society of Mechanical Engineers.

Zhang, W., Tung, Y., Johnsson, F., 1991. Radial voidage profiles in fast fluidized beds of different diameters. Chem. Eng. Sci. 46 (12), 3045–3052.

Zhang, W., Johnsson, F., Leckner, B., 1995. Fluid-dynamic boundary layers in CFB boilers. Chem. Eng. Sci. 50 (2), 201–210.

Zheng, W., Zhang, M., Zhang, Y., Lyu, J., Yang, H., 2019. The effect of the secondary air injection on the gas–solid flow characteristics in the circulating fluidized bed. Chem. Eng. Res. Des. 141, 220–228.